

# Helical Networks of $\pi$ -Conjugated Rods – A Robust Design Concept for Bicontinuous Cubic Liquid Crystalline Phases with Achiral $Ia\bar{3}d$ and Chiral $I23$ Lattice

Christian Dressel, Tino Reppe, Silvio Poppe, Marko Prehm, Huanjun Lu, Xiangbing Zeng, Goran Ungar,\* and Carsten Tschierske\*

Bicontinuous cubic liquid crystalline phases of  $\pi$ -conjugated molecules, representing self-assembled 3D-ordered interpenetrating networks with cubic symmetry, are receiving increasing attention due to their capacity for charge transport in all three dimensions and their inherent spontaneous helicity. Herein, a robust general design concept for creating bicontinuous cubic phases is reported. It is based on a nonsymmetric-substituted  $\pi$ -conjugated 5,5'-diphenyl-2,2'-bithiophene platform with one end containing three out-fanning flexible chains and with a range of substituents at the other end (the apex). The cubic phases are stable over broad temperature ranges, often down to ambient temperature, and tolerate a wide range of apex substitution patterns, allowing structural diversity and tailoring of the cubic phase type and application-relevant properties. With an increasing number and size of apex substituents, a sequence of three different modes of cubic self-assembly is observed, following an increasing helical twist. Thus, two ranges of the achiral double network  $Ia\bar{3}d$  phase range can be distinguished, a long pitch and a short pitch, with the chiral triple network  $I23$  cubic phase in the intermediate pitch range. The findings provide a new prospect for the directed design of cubic phase-forming functional materials based on spontaneously formed helical network liquid crystals with tunable application specific properties.

represent self-assembled supramolecular networks of branched columns which occur in soft matter systems at the transition from lamellar to columnar self-assembly.<sup>[4,5]</sup> They are known for amphiphilic<sup>[6–8]</sup> and dendritic<sup>[9]</sup> molecules and for macromolecules<sup>[10]</sup> in the liquid crystalline (LC) phases of the bulk materials<sup>[11–21]</sup> and the corresponding lyotropic systems with appropriate solvents (in lyotropics abbreviated as  $Cub_V$  phases).<sup>[7,22]</sup> They find applications for encapsulation of biological and bioactive molecules in drug delivery (cubosomes<sup>[23]</sup>), gene transfection, and protein crystallization,<sup>[24]</sup> as templates for the preparation of inorganic porous materials,<sup>[25]</sup> as selective membranes,<sup>[26]</sup> photonic and optical bandgap materials,<sup>[27,28]</sup> and many other.<sup>[5,29]</sup> Presently, they are receiving increasing interest as electron and ion conducting materials<sup>[30–37]</sup> with the unique feature of having conduction pathways in all three spatial directions.<sup>[38–45]</sup>  $Cub_{bi}$  phases of molecules involving  $\pi$ -conjugated rods and organized


in helical networks might also become of potential interest for circularly-polarized aggregation-induced emission for applications in a wide range of technologically important fields.<sup>[46–48]</sup>

In the  $Cub_{bi}$  phases there are one, two, or three continuous networks in a continuum between them, i.e., “bicontinuous” stands for (continuous) networks + continuum, irrespective of

## 1. Introduction

Networks are indispensable for information technology, intelligence, and open-end development of complex systems,<sup>[1,2]</sup> and covalently connected molecular networks form the basis of reticular chemistry.<sup>[3]</sup> Bicontinuous cubic phases ( $Cub_{bi}$ )

Dr. C. Dressel, T. Reppe, Dr. S. Poppe, Dr. M. Prehm, Prof. C. Tschierske  
Institute of Chemistry  
Martin Luther University Halle-Wittenberg  
Kurt-Mothes-Strasse 2, Halle/Saale D-06120, Germany  
E-mail: carsten.tschierske@chemie.uni-halle.de

 The ORCID identification number(s) for the author(s) of this article can be found under <https://doi.org/10.1002/adfm.202004353>.

© 2020 The Authors. Published by Wiley-VCH GmbH. This is an open access article under the terms of the Creative Commons Attribution License, which permits use, distribution and reproduction in any medium, provided the original work is properly cited.

<sup>[†]</sup>Present address: Jiangsu Key Laboratory of Advanced Functional Polymer Design and Application, Soochow University, Suzhou 215123, P. R. China

Dr. H. Lu,<sup>[†]</sup> Dr. X. Zeng, Prof. G. Ungar  
Department of Materials Science and Engineering  
University of Sheffield  
Sheffield S1 3JD, UK  
E-mail: g.ungar@sheffield.ac.uk

Prof. G. Ungar  
State Key Laboratory for Mechanical Behavior of Materials  
Shaanxi International Research Center for Soft Materials  
Xi'an Jiaotong University  
Xi'an 710049, China

DOI: 10.1002/adfm.202004353

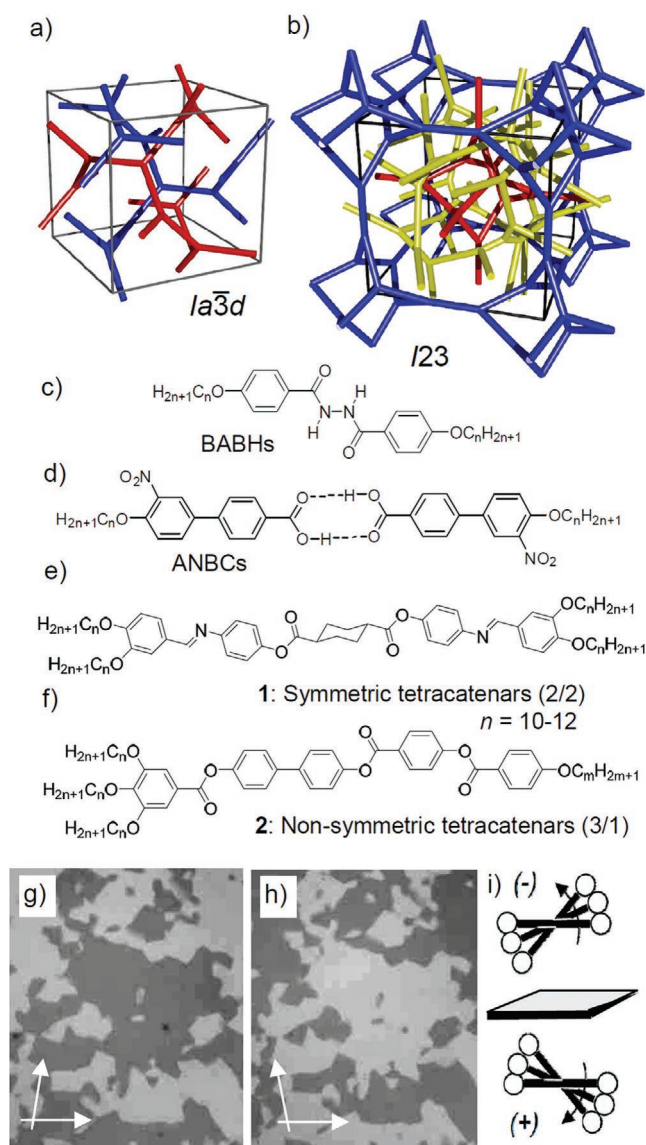


**Figure 1.** The  $Cub_{bi}$  phases formed by rod-like compounds; a) the double gyroid ( $Ia\bar{3}d$ ) involving two networks and b) the  $I23$  phase formed by three networks;<sup>[87,99]</sup> c–f) representative examples for the major classes of rod-like compounds forming these two types of  $Cub_{bi}$  phases; g, h) chiral conglomerate of the  $I23$  phase of  $3/351_2$  as observed upon cooling at  $T = 125$  °C between slightly uncrossed polarizers (contrast enhanced); the width of both images is 0.5 mm; i) the helical twist developing along the networks due to the clashing of the bulky end groups between the molecules organized in the networks shown in (a, b).

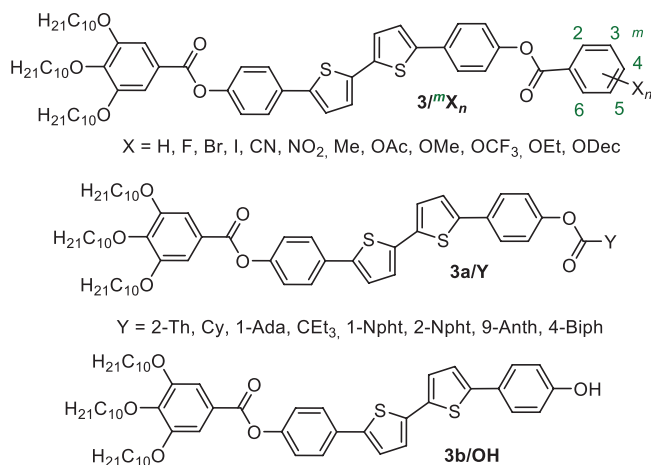
how many networks there are.<sup>[49]</sup> In the most common case, two interwoven networks with three way junctions are organized in a  $Ia\bar{3}d$  lattice (the double gyroid, **Figure 1a**), which is the most frequently observed type of  $Cub_{bi}$  phase.<sup>[7,14,17]</sup> However, as soon as rod-like segments are included in the molecular structure (Figure 1c–f), new cubic and also noncubic network phases can be observed.<sup>[50–65]</sup> In most cases, these rods are organized in the networks and on average lie perpendicular to the network segments.<sup>[14–17,66]</sup> For these  $Cub_{bi}$  phases, beside the  $Ia\bar{3}d$  phase, a second more complex type of cubic phase with a larger

lattice parameter was found.<sup>[13,14,16,67–80]</sup> In early works, it was assigned to the  $Im\bar{3}m$  space group and models involving three minimal surfaces,<sup>[52,81]</sup> three networks,<sup>[82,83]</sup> or combining two networks with additional spherical aggregates<sup>[84,85]</sup> were proposed. Recently, the observation of spontaneous mirror symmetry breaking and formation of chiral conglomerates in this “ $Im\bar{3}m$ ” phase, and occasionally also in the adjacent isotropic liquid phase (Iso<sub>1</sub><sup>[x]</sup>)<sup>[86]</sup> provoked significant interest in this kind of cubic phase and provided a breakthrough in the understanding of its self-assembly. It was shown that in all cases, the “ $Im\bar{3}m$ ” phase is intrinsically chiral, whereas the double gyroid ( $Ia\bar{3}d$ ) is always achiral.<sup>[87–94]</sup> This was explained by a helical organization of the molecules in the networks of these cubic phases. The helix formation is the result of steric repulsion between the end chains of the almost parallel aligned rod-like molecules, requiring a slight twist between the molecules along the network segments (see Figure 1i).<sup>[95,96]</sup> In the  $Ia\bar{3}d$  phase, there are two networks in which the helical sense is opposite (Figure 1a),<sup>[87,97,98]</sup> and therefore it is optically inactive. By contrast, the “ $Im\bar{3}m$ ” phase is composed of three networks (Figure 1b), where the chirality cannot cancel out, leading to a unichiral structure with macroscopic chirality expressed by conglomerate formation (see, for example, Figure 1g, h).<sup>[87]</sup> Due to the proven chirality, the space group of this triple network phase cannot be  $Im\bar{3}m$ ,<sup>[52,82,83]</sup> and recently a model with chiral  $I23$  space group was proposed, where all three nets have three-fold junction as known for the double gyroid (Figure 1b).<sup>[99]</sup>

However, the formation of  $Cub_{bi}$  phases is in general extremely sensitive to slight modifications of the molecular structure, easily leading to transition to the adjacent lamellar or columnar phases.<sup>[11–16]</sup> Therefore,  $Cub_{bi}$  phases are usually not predictable and appear only in narrow temperature ranges for few well designed compounds (Figure 1c–f). The most prominent are rod-like hydrogen bonded dimers of 4'-n-alkoxy-3'-nitrobiphenyl-4-carboxylic acids (ANBCs),<sup>[100–104]</sup> the dibenzoyldiazines (BABHs)<sup>[105–111]</sup> (Figure 1c, d),<sup>[16,17,108,110]</sup> and tetracatenar molecules, which can have either a symmetric or a nonsymmetric distribution of the alkyl chains (Figure 1e, f).<sup>[112–124]</sup> Nevertheless, even these compounds are very sensitive to minor molecular structural variations. For example, only the  $NO_2$ - and CN-substituted biphenyl carboxylic acids (Figure 1d) form  $Cub_{bi}$  phases, whereas the nonsubstituted or related halogenated compounds do not.<sup>[125]</sup> Likewise, symmetric tetracatenars with any substituent (e.g.,  $CH_3$ , F, CN) replacing only one H-atom at the core unit do not form any  $Cub_{bi}$  phase.<sup>[116]</sup> Therefore, it is presently not possible to efficiently tailor the phase type and application relevant properties (e.g., band gap) of these compounds by molecular design.

Herein, we introduce the concept of taper-shaped tetracatenars (3/0 tetracatenars;  $m/n$  gives the number of alkyl chains at each end of the rod) as a general design concept for robust  $Cub_{bi}$  phase-forming materials which can be modified by a wide range of substituents at the apex (**Scheme 1**). This makes it possible to tailor the cubic phase type and the electronic properties of the  $\pi$ -conjugated molecules in question. It is also shown that this can be used to steer the helical networks involved in the  $Cub_{bi}$  phase to either a chiral ( $I23$ ) or an achiral  $Cub_{bi}$  phase ( $Ia\bar{3}d$ ).

To this end, the taper-shaped tetracatenar compounds  $3/mX_n$  and  $3a/Y$  were synthesized (Scheme 1). These compounds involve a  $\pi$ -conjugated 5,5'-diphenyl-2,2'-bithiophene rod



**Scheme 1.** Chemical structures of the polycatenar bithiophene derivatives  $3^mX_n$  and  $3a/Y$  under consideration.

providing potential application relevant functional properties.<sup>[126–128]</sup> They are terminated at one end by a 3,4,5-tridecyloxybenzoyloxy group and at the opposite end, referred to as apex, by a series of systematically varied substituents to adjust their capability to self-assemble in network structures with cubic symmetry. In the series of compounds  $3^mX_n$ , the apex is a benzoate unit and the position of the substituent(s) at this unit is indicated by superscripts ( $m$ ) before  $X$  and the number of substituents is added as a subscript ( $n$ ) after  $X$ , e.g.,  $3^{35}I_2$  means two iodines in positions 3 and 5. In compounds  $3a/Y$ , the benzene ring at the apex is replaced by other aromatic, heteroaromatic, alicyclic, or branched units  $Y$ .

## 2. Experimental Section

### 2.1. Synthesis

The synthesis of the tricatener phenol **3b/OH** (Scheme 1) was conducted by Suzuki type boronate cross-coupling reactions, as reported previously.<sup>[86]</sup> Acylation of **3b/OH** with appropriate benzoyl chlorides led to the compounds  $3^mX_n$  and  $3a/Y$ , as described in the Supporting Information.

### 2.2. Investigation Methods

Investigation of the obtained materials was conducted by polarizing optical microscopy (POM) (Optiphot 2, Nikon microscope with a Mettler FP82HT heating stage), differential scanning calorimetry (DSC-7 and DSC-8000 Perkin Elmer, 10 K min<sup>-1</sup> peak temperatures quoted in Table S1 in the Supporting Information), and X-ray diffraction (XRD). In-house XRD was carried out using Cu<sub>Kα</sub> radiation and a Vantec 500 area detector. High-resolution small-angle X-ray scattering patterns were recorded at beamline I22 of Diamond Light Source with a Pilatus 2M detector and at XmaS beamline B28 of the European Synchrotron Radiation Facility (ESRF). Powder samples in capillaries were temperature controlled with a Linkam hot stage.

## 3. Results and Discussion

### 3.1. Characterization of the Cubic Phases

The cubic phases appear uniformly dark between fully (90°) crossed polarizers as they are optically isotropic. The transition from the isotropic liquid (Iso) to the cubic phases was identified by the sudden increase of viscosity associated with a DSC peak with  $\Delta H = 2\text{--}5$  kJ mol<sup>-1</sup>. Usually, there is a 5–12 K supercooling of the Iso–Cub transition relative to the Cub–Iso transition temperature on heating (Tables S1 and S2 in the Supporting Information for numerical data and Figures S1 and S14a in the Supporting Information for representative DSC traces). Polarizing microscopy allows an easy preliminary discrimination between the two cubic phase types formed by rod-like molecules, the  $Ia\bar{3}d$  and  $I23$  phases. The achiral  $Ia\bar{3}d$  phase remains uniformly dark also after rotating one of the polarizers by a small angle out of the fully crossed orientation. By contrast, the mirror symmetry broken  $I23$  phase shows a conglomerate of dark and bright domains after slight rotation of one polarizer by 1°–10° either clockwise or counterclockwise (Figure 1g,h).

For further confirmation, the cubic phases were investigated by XRD. The powder diffraction pattern of the  $Ia\bar{3}d$  phase is characterized by the well resolved (211) and (220) reflections, whereas for  $I23$  a characteristic pattern of the dominating (321) with a shoulder for the (400) reflection and a small (420) reflection is observed (Figure S9 and Tables S3 and S4, Supporting Information). Representative examples were investigated using a synchrotron source (Figures S10–S12 and Tables S5–S9, Supporting Information). The high resolution XRD pattern of the cubic  $Ia\bar{3}d$  and  $I23$  phases of compound  $3^3F$  and  $3^{35}F_2$ , respectively, are shown in Figure 2a,c. The electron density (ED) maps of these two cubic phases, reconstructed on the basis of the diffraction intensities (Figure 2b,d) show the double gyroid structure of the  $Ia\bar{3}d$  phase and the complex triple network structure of the  $I23$  phase. Details of the reconstruction are described in the Supporting Information, and for details of the ED reconstruction in the case of the non-centrosymmetric  $I23$  phase, see also ref. [99].

### 3.2. Tailoring of the Cubic Phases of the Tricatener $3^mX_n$ by Apex Substituents

#### 3.2.1. 4-Substituted Compounds

Figure 3a shows the effect of increasing the size of apex substitution in the terminal 4-position with respect to the COO group (compounds  $3^4X$ ). As shown, even for large substituents, like iodine and OCF<sub>3</sub>, the Cub<sub>bi</sub> phase is retained over a wide temperature range. It should be noted that the transition temperatures in Figure 3a and all following bar diagrams were measured on heating and the observed LC phases represent thermodynamically stable (enantiotropic) phases, whereas on cooling, much broader metastable cubic ranges, often down to ambient temperature, were observed (see Table S1 in the Supporting Information).

Interestingly, the stability and the phase range of the Cub<sub>bi</sub> phase is enlarged by increasing the size of the substituent

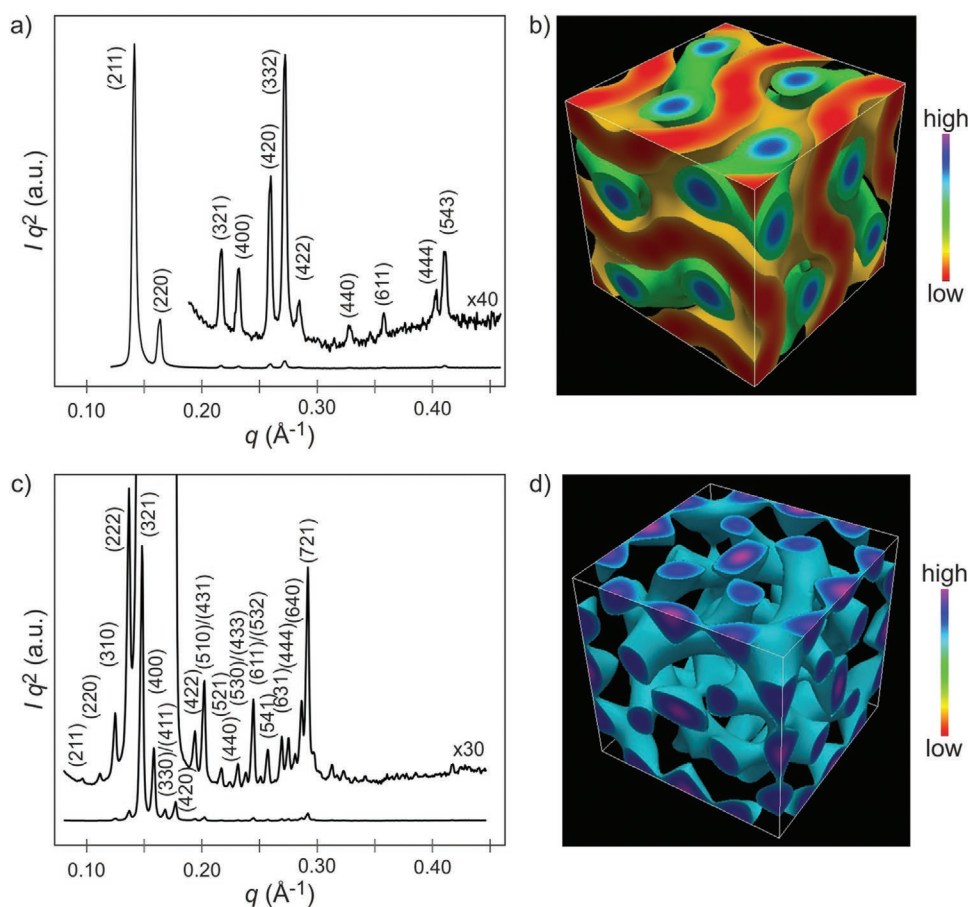


**Figure 2.** a) XRD pattern (recorded at 125 °C) and b) the reconstructed electron density map of the  $Ia\bar{3}d$  cubic phase formed by compound  $3/3^3F$ . In the electron density map, the green isoelectron surface encloses the highest 25% of the total volume, while the orange isoelectron surface encloses the lowest 50% of the unit cell volume. c) XRD pattern recorded at 125 °C and d) the electron density map of the  $I23$  cubic phase formed by compound  $3/3^3F_2$ . The light blue isoelectron surface encloses the higher 25% of the unit cell volume, showing the triple network structure. Vertically expanded diffractograms were added in (a) and (c) to show weaker diffraction peaks; labeled by their Miller indices.

( $H < F < I$ ), whereby electron acceptors (halogens,  $OCF_3$ ,  $CN$ ,  $NO_2$ ), reducing the electron density of the polyaromatic core, have a larger stabilizing effect than donors ( $CH_3$ ,  $OCH_3$ ) with approximately the same volume. This becomes especially evident if  $3/4^3CN$  and  $3/4^3Me$ , both having the same volume of the substituent, but very different Hammett substituent constants (as measures for the electronic substituent effects)<sup>[129]</sup> are compared (Table 1). Table 1 also summarizes the volumes of the different substituents as estimated using crystal volume increments ( $V_c$ )<sup>[130]</sup> and their Hammett constants ( $\sigma_m$ ,  $\sigma_p$ )<sup>[129]</sup>. In most cases, the  $Cub_{bi}$  phase of the 4-substituted compounds is  $Ia\bar{3}d$ , only for the  $OCF_3$  group, the phase type changes to  $I23$ .<sup>[131]</sup> The cubic lattice parameter  $a_{cub}$  of the  $Ia\bar{3}d$  phase of all 3/0 type tricatener compounds  $3/4^3X$  is in the same range between 10.8 and 11.5 nm (Table 1 and Table S1 (Supporting Information)) and only slightly increasing with the volume of the substituent X, whereas that of the  $I23$  phase of  $3/4^3OCF_3$  is about one half larger ( $a_{cub} = 16.2$  nm), in line with the triple network structure. Compound  $3/4^3ODec$ , also forming the  $I23$  phase but belonging to the 3/1-tetracatenar compounds, will be discussed further below.

### 3.2.2. 3-Substituted Compounds

Shifting the substituent X to the lateral 3-position (Figure 4a) provides reduced  $Cub$ – $Iso$  transition temperatures compared to the 4-substituted compounds; only the polar electron acceptor substituents F, Br and especially CN can still stabilize the cubic phase compared to  $X = H$ . This cubic phase stabilizing effect of polar substituents is smaller than for the 4-substituted series, due to the competing effect of the stronger steric distortion of molecular packing by the lateral position of the substituents. The cubic phase stabilizing effect of the polar CN group is again outstanding if compared with Br, having a similar volume. The  $Cub_{bi}$  phase type changes already for  $X = Br$  from  $Ia\bar{3}d$  to  $I23$ , indicating the stronger steric effect of the substituents in the lateral 3-position on the phase type (Figure 4a and Table 2). Only for compound  $3/3^3OEt$ , the  $I23$  phase is observed under all conditions, whereas for compounds  $3/3^3OMe$ ,  $3/3^3Br$ , and  $3/3^3I$ , both  $Cub_{bi}$  phase types,  $Ia\bar{3}d$  and  $I23$ , can be found depending on temperature and other conditions such as cooling rate and thermal history (for a more detailed discussion, see Section S1.4 in the Supporting Information). Overall, with increasing

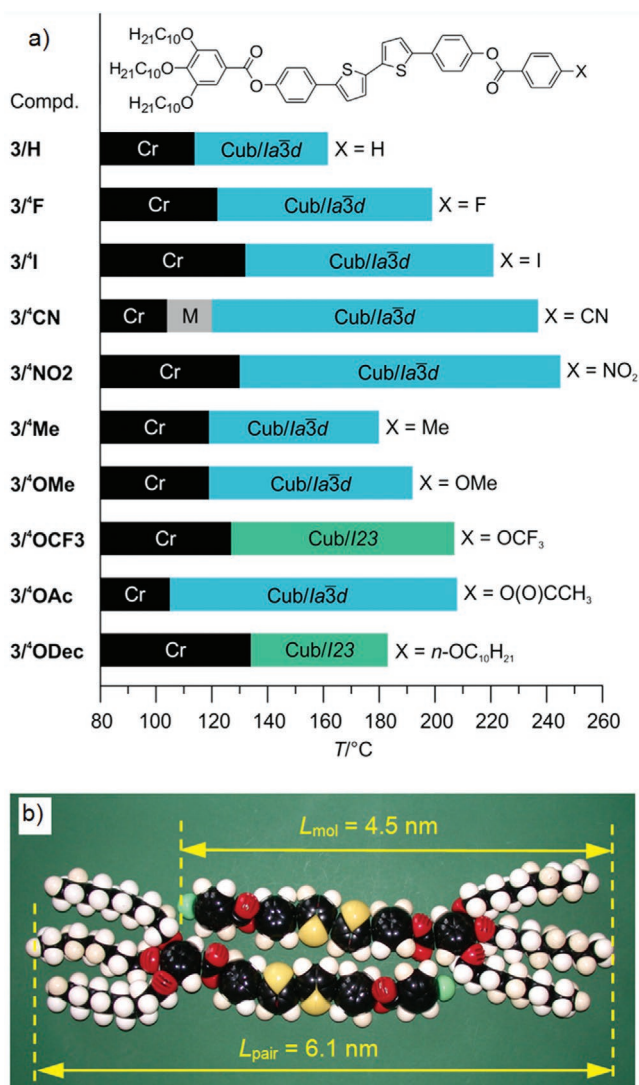


**Figure 3.** a) Mesophases and transition temperatures of compounds  $3^i/X$  as observed on heating; for the numerical data of the transitions on heating and cooling, including transition enthalpy values of  $3^i/H$  and  $3^i/ODec$ , added for comparison, see ref. [87]; for all other compounds, see Table S1 in the Supporting Information; abbreviations: Cr = crystalline solid  $Cub/la\bar{3}d = Cub_{bi}$  phase with  $la\bar{3}d$  lattice; all  $la\bar{3}d$  phases represent long pitch  $la\bar{3}d_{(L)}$  phases;  $Cub/I23 = Cub_{bi}$  phase with  $I23$  lattice, M = unknown mesophase, the isotropic liquid state (Iso) is at the right side of the columns; b) space filling molecular models (CPK models) of the proposed organizations of the molecules of compound  $3^i/F$  in the  $Cub_{bi}$  phase.

volume of X there is a transition from  $la\bar{3}d$  (X = H, F) via an  $I23-la\bar{3}d$  dimorphism (X = Br, I, OMe) to  $I23$  (X =  $OC_2H_5$ ). In the sequence  $OCH_3-OC_2H_5-OC_{10}H_{21}$ , i.e., by elongation of the alkoxy chain (Figure 4a), the  $la\bar{3}d$  phase is at first completely removed and replaced by the  $I23$  phase for  $OC_2H_5$  and then the  $la\bar{3}d$  phase re-emerges for  $OC_{10}H_{21}$ . Thus, there appear to be two  $la\bar{3}d$  phase ranges, one favored at small apex size and the second one requiring a significantly larger substituent at the apex; the two are separated by the  $I23$  phase for medium effective volume of the substituent X. The transition from  $3^i/3^iOMe$  to  $3^i/3^iODec$  (and from  $3^i/3^iOMe$  to  $3^i/3^iODec$ , see Figure 3a) can

**Table 1.** Dependence of lattice parameter  $a_{cub}$  and other structural parameters on the volume of the substituent X ( $V_{CX}$ ) in the compounds  $3^i/X$ .

Compounds <sup>a)</sup>	$V_{CX} [\times 10^{-3} \text{ nm}^3]$	$\sigma_m$	$\sigma_p$	$Cub_{bi}$	$a_{cub} [\text{nm}]$	$n_{raft}$	$\Phi [^\circ]$
$3^i/H$	6.9	–	–	$la\bar{3}d_{(L)}$	10.8	3.9	8.3
$3^i/F$	12.8	0.34	0.06	$la\bar{3}d_{(L)}$	11.1	4.0	8.1
$3^i/I$	25.6	0.71	0.78	$la\bar{3}d_{(L)}$	11.1	4.0	8.1
$3^i/CN$	31.3	0.56	0.66	$la\bar{3}d_{(L)}$	11.2	4.0	8.0
$3^i/Me$	31.7	–0.07	–0.17	$la\bar{3}d_{(L)}$	11.4	4.2	7.9
$3^i/I$	45.0	0.35	0.18	$la\bar{3}d_{(L)}$	11.3	4.1	7.9
$3^i/OMe$	46.3	0.12	–0.27	$la\bar{3}d_{(L)}$	11.4	4.2	7.9
$3^i/OAc$	58.6	0.39	0.31	$la\bar{3}d_{(L)}$	11.5	4.1	7.8
$3^i/OCF_3$	58.6	0.38	0.35	$I23$	16.2	3.4	8.6

<sup>a)</sup>  $V_{CX}$  = crystal volume of the substituent X, estimated with the crystal volume increments ( $V_c$ ) reported by Immirzi and Perini;<sup>[130]</sup>  $\sigma_m$  and  $\sigma_p$  are Hammett constants (Table S11, Supporting Information);<sup>[129]</sup>  $\sigma_m$  is a measure of the strength of electron withdrawing (+) and electron donating (–) effects via the  $\sigma$  bonds (inductive effect) and  $\sigma_p$  is an analogous measure for the delocalization of the  $\pi$ -electrons (resonance effect); large positive values of  $\sigma_m$  and  $\sigma_p$  indicate electron acceptors, whereas small positive and negative values are typically found for electron donating substituents;  $n_{raft}$  = number of molecules organized in each 0.45 nm thick raft of the networks, calculated as described in Table S10 (Supporting Information);  $\Phi$  = helical twist between adjacent 0.45 nm thick rafts of molecules along the networks, calculated according to:  $\Phi(la\bar{3}d) = 70.5^\circ/[0.354a_{cub}/0.45 \text{ nm}]^{[87]}$  and  $\Phi(I23) = 90^\circ/[0.290a_{cub}/0.45 \text{ nm}]^{[99]}$  abbreviations:  $la\bar{3}d_{(L)}$  = long pitch  $la\bar{3}d$  phase;  $I23 = Cub_{bi}/I23$  phase.

be considered as a transition between two types of polycatenars, the taper-shaped 3/0 tricatens and the nonsymmetric 3/1 tetracatenars.<sup>[132]</sup>

As shown in Figure 5a,b, this phase sequence is also observed by POM in the contact region between the achiral  $la\bar{3}d$  phases of  $3^i/H$  and  $3^i/3^iODec$  where a ribbon of the chiral  $I23$  phase is induced. Thus, tailoring of the cubic phase structure and mirror symmetry breaking is not only achievable by the design of individual compounds, but also by mixing compounds with different sizes of the substituents.<sup>[111,117]</sup>

### 3.2.3. 3,5-Disubstituted Compounds

The 3,5-disubstitution pattern (Figure 4b) provides an even stronger steric effect than only one 3-substituent, and therefore in all cases, even for X = F, the  $la\bar{3}d$  phase of  $3^i/H$  is replaced by the  $I23$  phase. Outstanding is again the effect of the polar electron accepting  $NO_2$  group, leading to the highest  $Cub_{bi}$ -Iso transition temperature and the widest cubic range despite its significant size. We attribute this phase stabilization to two main effects. First, the increased dipole moment strengthens the electrostatic intermolecular interactions. Especially, the stronger core–core interaction between the electron-deficient apex and the trialkoxy-substituted electron donor ends in an antiparallel side-by-side packing of the polyaromatic rods (Figure 3b) leads to a denser packing, stabilizing the networks. Second, the polar groups increase the incompatibility of the polyaromatic core units with the nonpolar aliphatic chains,

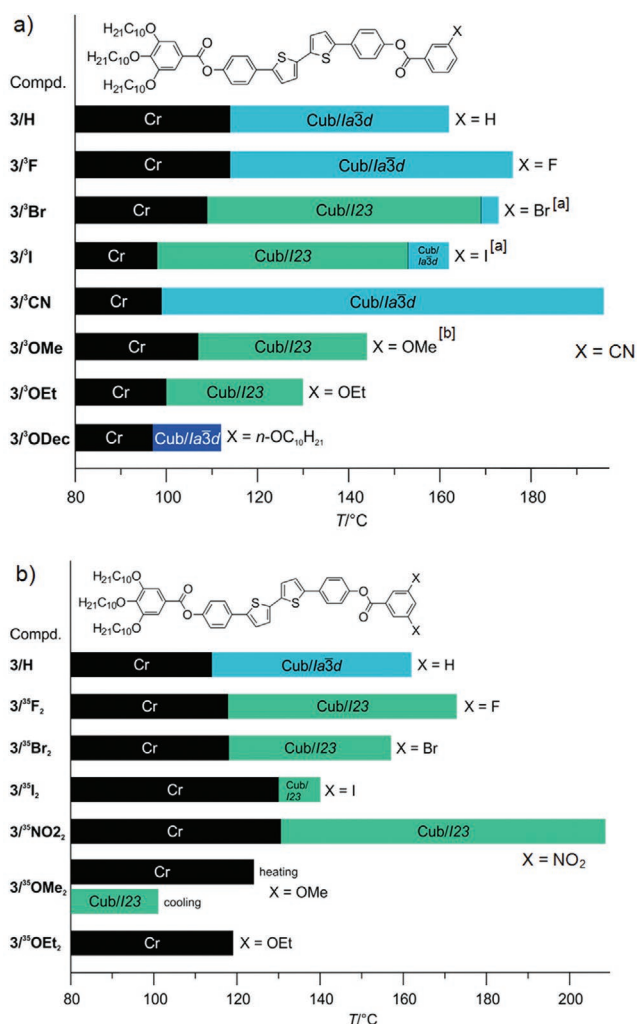


**Figure 4.** Mesophases and transition temperatures a) of compounds  $3/3^3X$  and b) of compounds  $3/3^{35}X_2$ , recorded on heating; for compound  $3/3^3\text{ODec}$ , a  $\text{Col}_{\text{hex}}$  phase is formed on cooling from Iso which is rapidly replaced by the  $Ia\bar{3}d$  phase (see Figure S2 in the Supporting Information); the  $Ia\bar{3}d$  phase of  $3/3^3\text{ODec}$ , indicated by a darker blue, represents a short pitch  $Ia\bar{3}d_{(S)}$  phase, whereas all others, shown in light blue belong to the long pitch  $Ia\bar{3}d_{(L)}$  type. <sup>[a]</sup> For  $3/3^3\text{Br}$  and  $3/3^3\text{I}$  only, the  $Ia\bar{3}d$  phase is observed on cooling; <sup>[b]</sup> for  $3/3^3\text{OMe}$  on cooling,  $Ia\bar{3}d$  and  $I23$  phases were observed, depending on the condition, see Section S1.4 in the Supporting Information; the numerical data are collated in Table S1 in the Supporting Information and for  $3/3^3\text{H}$  and  $3/3^3\text{OEt}$ , see ref. [87].

additionally contributing to mesophase stability by strengthened segregation.<sup>[15,16,133]</sup> In both series  $3/3^3X$  and  $3/3^{35}X_2$ , there is no significant effect of the volume of the apex on the lattice parameter, it being 15.6–16.4 nm for the  $I23$  phase and 10.4–10.9 nm for the  $Ia\bar{3}d$  phase (Table 2). Only the  $Ia\bar{3}d$  lattice of  $3/3^3\text{ODec}$  has a significantly smaller size ( $a_{\text{cub}} = 9.8$  nm) despite the fact that this compound has the largest and the longest substituent. In the fully intercalated antiparallel organization, the additional long alkyl chain is organized between the other alkyl chains. In this arrangement, the length of the pairs is not changed, but the number of alkyl chains in the periphery grows and this reduces the number of molecules in the network cross-section, which then reduces  $a_{\text{cub}}$ .

**Table 2.** Dependence of lattice parameter  $a_{\text{cub}}$  and other packing parameters on the volume of the apex ( $V_{\text{apex}}$ ) of compounds  $3/3^mX_n$  and  $3a/Y$ .

Compounds <sup>a)</sup>	$V_{\text{apex}}$ [nm <sup>3</sup> ]	Cub	$a_{\text{cub}}$ [nm]	$n_{\text{raft}}$	$\Phi$ [°]
$3/3^3\text{H}$	0.11	$Ia\bar{3}d_{(L)}$	10.8	3.9	8.3
$3/3^3\text{F}$	0.12	$Ia\bar{3}d_{(L)}$	10.9	3.9	8.2
$3/3^{35}\text{F}_2$	0.12	$I23$	15.8	3.3	8.8
$3/3^3\text{CN}$	0.13	$Ia\bar{3}d_{(L)}$	10.8	3.7	8.3
$3/3^3\text{Br}$	0.14	$Ia\bar{3}d_{(L)}$ $I23$	10.4 16.4	3.5 3.5	8.6 8.5
$3/3^{35}\text{NO}_2$	0.15	$I23$	15.8	3.3	8.8
$3/3^3\text{I}$	0.15	$Ia\bar{3}d_{(L)}$ $I23$	n.d. 16.2	– 3.4	– 8.6
$3/3^3\text{OMe}$	0.15	$Ia\bar{3}d_{(L)}$ $I23$	10.8 16.1	3.7 3.4	8.3 8.7
$3/3^{35}\text{Br}_2$	0.15	$I23$	16.1	3.3	8.7
$3/3^3\text{OEt}$	0.18	$I23$	15.7	3.2	8.9
$3/3^{35}\text{I}_2$	0.19	$I23$	15.6	3.1	9.0
$3/3^3\text{ODec}$	0.37	$Ia\bar{3}d_{(S)}$	9.8	2.7	9.1
$3/3^{345}\text{F}_3$	0.13	$I23$	15.6	3.2	9.0
$3/3^{23456}\text{F}_5$	0.14	$I23$	15.6	3.2	9.0
$3/3^{345}\text{OMe}$	0.21	$I23$	15.4	2.9	9.1
$3a/\text{Cy}$	0.14	$I23$	15.6	3.2	9.0
$3a/\text{Ad}$	0.22	$I23$	15.1	2.8	9.2
$3a/\text{CEt}_3$	0.18	$Ia\bar{3}d_{(S)}$	8.9	2.4	10.1
$3a/1\text{-Npht}$	0.20	$Ia\bar{3}d_{(L)}$	10.6	3.5	8.5
$3a/2\text{-Npht}$	0.20	$Ia\bar{3}d_{(L)}$	11.6	4.2	7.7
$3a/\text{Biph}$	0.21	$Ia\bar{3}d_{(L)}$	12.0	4.4	7.5

<sup>a)</sup> Abbreviations:  $Ia\bar{3}d_{(S)}$  = short pitch  $Ia\bar{3}d$  phase; for the other abbreviations, see Figure 1 and Table 1;  $V_{\text{apex}}$  includes the benzene ring with attached substituents X ( $3/3^mX_n$ ) or the group Y ( $3a/Y$ ); for calculations, see Table S10 in the Supporting Information.

The total length of the networks in each unit cell ( $L_{\text{net}}$ ) can be calculated according to  $L_{\text{net}} = 8.485a_{Ia\bar{3}d}$  for the  $Ia\bar{3}d$  phase<sup>87</sup> and according to  $L_{\text{net}} = 20.68a_{I23}$  for the  $I23$  phase,<sup>[99]</sup> and the number of molecules arranged along this distance is determined by  $L_{\text{net}}/n_{\text{cell}}$ , where  $n_{\text{cell}}$  is the number of molecules per unit cell. Assuming a constant distance between the molecules of 0.45 nm, it is calculated according to  $n_{\text{raft}} = n_{\text{cell}}/(L_{\text{net}}/0.45)$  that about four ( $n_{\text{raft}} = 3.9$ ) molecules are organized in the rafts forming the networks of  $3/3^3\text{H}$  and only about three ( $n_{\text{raft}} = 2.7$ ) for  $3/3^3\text{ODec}$  (see Table 2). This means that peripheral space filling reduces the diameter of the network segment, which additionally affects the inter-raft twist. In the  $Ia\bar{3}d$  phase, the twist between the molecules in neighboring rafts can be calculated according to  $\Phi(Ia\bar{3}d) = 70.5^\circ/[0.354a_{\text{cub}}/0.45 \text{ nm}]^{[87]}$  and in the  $I23$  phase as  $\Phi(I23) = 90^\circ/[0.290a_{\text{cub}}/0.45 \text{ nm}]^{[99]}$  Table 2 collates the lattice parameters  $a_{\text{cub}}$  and the twist angles  $\Phi$  of compounds  $3/3^3X$  and  $3/3^{35}X_2$  depending on the total volume of the substituted benzene ring at the apex ( $V_{\text{apex}}$ ). Interestingly, the calculated twist angle  $\Phi$  continuously rises with expanding apex volume across the  $Ia\bar{3}d \rightarrow I23 \rightarrow Ia\bar{3}d$  transitions from  $8.2^\circ$  to  $8.6^\circ$  in  $Ia\bar{3}d$  via  $8.5^\circ$ – $9.0^\circ$  in  $I23$  to  $9.1^\circ$  for the  $Ia\bar{3}d$  phase of  $3/3^3\text{ODec}$ . This means that with increasing size of the

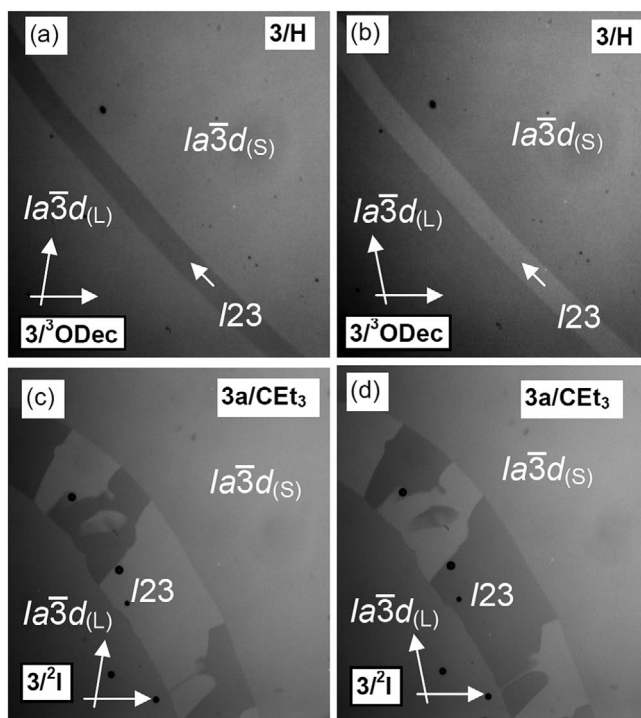
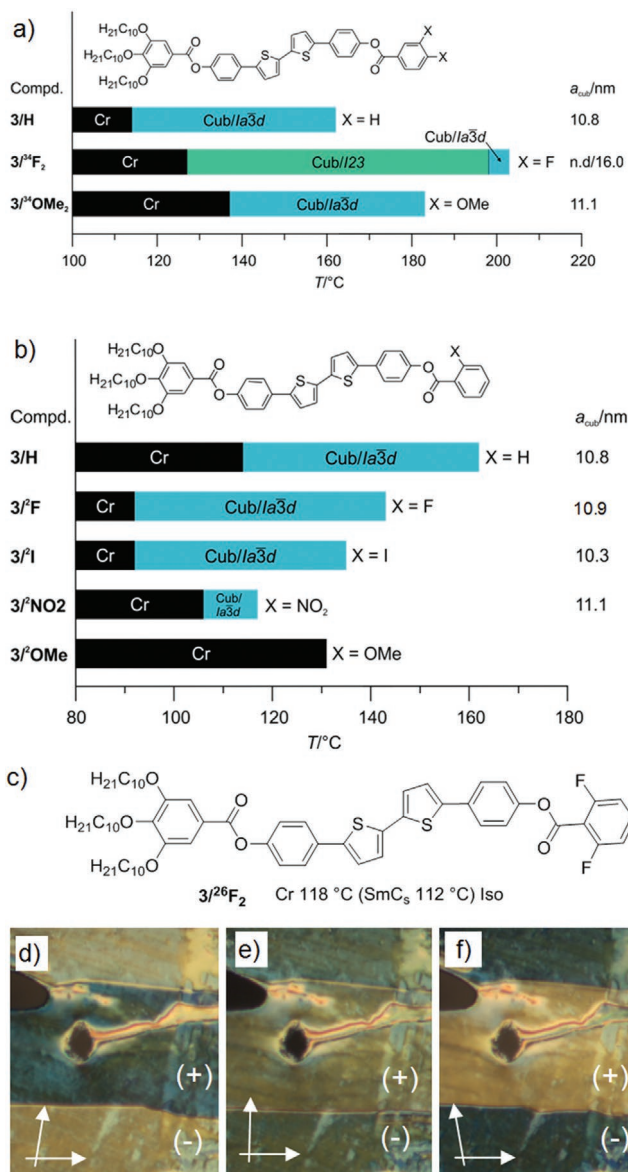


**Figure 5.** Ribbon of the chiral  $I23$  phase developing in the contact region between the achiral  $Ia\bar{3}d$  phases of a,b)  $3/H$  (top/right) and  $3/3^{\text{O}Dec}$  (bottom/left) as observed at  $T = 104^{\circ}\text{C}$  (on cooling, the  $I23$  phase is formed below  $124^{\circ}\text{C}$  and on heating, it disappears at  $141^{\circ}\text{C}$ ) and c,d)  $3a/CEt_3$  (top/right) and  $3/1$  (bottom/left) as observed at  $T = 115^{\circ}\text{C}$  (on cooling, the  $I23$  phase is formed below  $117^{\circ}\text{C}$  and on heating, it disappears at  $132^{\circ}\text{C}$ ) after uncrossing the polarizer and analyzer in opposite directions; contrast enhanced, the width of the images is  $0.5\text{ mm}$ .

apex, the helical twist becomes larger and the pitch becomes shorter and therefore a frustration between pitch length and the distance between the junctions arises in the  $Ia\bar{3}d$  phase. At a certain degree of frustration, the  $Ia\bar{3}d$  phase is replaced by the triple network structure with  $I23$  lattice, allowing a larger twist angle  $\Phi$ . However, this advantage of the  $I23$  lattice obviously exists only for a certain range of the helical pitch and upon further increasing the volume of the apex, a mismatch arises also in  $I23$ . The  $I23$  phase appears to be even more sensitive to any mismatch between junction distance and pitch length and after reaching this limit, the  $Ia\bar{3}d$  lattice becomes the thermodynamically more stable mode of self-assembly again. This means that there is a long pitch ( $Ia\bar{3}d_{(L)}$ ) and a short pitch  $Ia\bar{3}d_{(S)}$  phase ( $Ia\bar{3}d_{(S)}$ ) which are separated by the  $I23$  phase.

### 3.2.4. 3,4-Disubstituted Compounds

In contrast to the 3,5-disubstitution pattern (Figure 4b), 3,4-disubstitution (Figure 6a) stabilizes the cubic phases by 30–40 K compared to the 3-monosubstituted, whereas the effect on the cubic phase type is weaker than for the 3,5 disubstitution pattern. For example, the  $I23$  phase of  $3/3^{\text{O}Me}$  is removed and the  $Ia\bar{3}d$  phase becomes dominant again for the 3,4-dimethoxy-substituted compound  $3/3^{\text{O}Me_2}$ . Because no induced  $I23$  phase could be found in the contact region between the  $Ia\bar{3}d_{(L)}$  phase of compound



### 3.2.5. 2-Substituted and 2,6-Disubstituted Compounds

As expected, the cubic phases are destabilized by the 2-substituents at the apex, due to their especially strong distorting steric effect on the molecular packing in this position (Figure 6b). The cubic phase stability is even for the fluorinated compound  $3/{}^2\text{F}$  and the 2-nitro-substituted compound  $3/{}^2\text{NO}_2$  reduced compared to  $3/\text{H}$ , and the 2-OMe-substituted compound  $3/{}^2\text{OMe}$  does not show any LC phase (melting point: 131 °C). The very different effect of 2-substitution by the  $\text{NO}_2$  group compared to 3-substitution becomes obvious by comparing Figures 4b and 6b. It appears that in 2-position, the mesophase stabilizing effect of this electron acceptor group is switched off and only the destabilizing steric effect remains. This might be due to a twist introduced around the COO group which hinders the electrostatic interaction with the sterically demanding trialkoxy-substituted donor ring in the antiparallel packing. That even in this case the  $\text{Cub}_{\text{bi}}$  phase is retained demonstrates clearly the robustness of the design concept of  $3/0$  tricaténars. While the 2-substitution strongly reduces the stability of the cubic phase, there is no change in the cubic phase type; even  $3/{}^2\text{I}$  forms exclusively the long pitch  $Ia\bar{3}d_{(\text{L})}$  phase, as confirmed by the induction of a chiral  $I23$  phase in the contact region with the  $Ia\bar{3}d_{(\text{S})}$  phase of  $3\text{a}/\text{CET}_3$  (Figure 5c,d). By contrast, for the isomeric laterally 3-substituted compound  $3/{}^3\text{I}$ , the  $I23$  phase dominates (Figure 4a).

Compound  $3/{}^{26}\text{F}_2$  having two *ortho*-fluorines in the 2- and 6-positions does not form any cubic phase. This compound melts at 118 °C and shows only a monotropic and synclitic tilted  $\text{SmC}_s$  phase on cooling below 112 °C (Figure 6c). A special feature of the  $\text{SmC}_s$  phase of  $3/{}^{26}\text{F}_2$  is the formation of chiral domains in thin homeotropically aligning cells, indicated by an optical texture showing a conglomerate of dark and bright domains inverting their brightness upon inverting the twist sense of the analyzer (Figure 6d–f) and remaining unchanged by rotation of the sample between crossed polarizers (Figure S4, Supporting Information).<sup>[134,135]</sup> In the case of compound  $3/{}^{26}\text{F}_2$ , the steric effects of the two *ortho*-fluorines can obviously stabilize helical conformers around the COO group,<sup>[136]</sup> thus supporting chirality synchronization by helix formation between the substrate surfaces.<sup>[137]</sup> Overall, substitution in the 2-position has a strong destabilizing effect on the  $\text{Cub}_{\text{bi}}$  phase without significantly affecting the cubic space group.

### 3.2.6. 3,4,5-Trisubstituted and 2,3,4,5,6-Pentasubstituted Compounds

The effect of 3,4,5-trisubstitution is shown in Figure 7 for F and OMe substituents as examples. Only the  $I23$  type  $\text{Cub}_{\text{bi}}$  phase is observed for both compounds. Again, the additional additional fluorine in the 4-position of the trisubstituted compound  $3/{}^{345}\text{F}_3$  enhances the cubic phase stability compared to the 3,5-disubstituted compound  $3/{}^{35}\text{F}_2$  by 25 K (Figure 4b). A similar stabilization is observed by comparing the methoxy-substituted compounds  $3/{}^{35}\text{OMe}_2$  (Figure 4b) and  $3/{}^{345}\text{OMe}_3$  (Figure 7). Even the pentafluorobenzoate  $3/{}^{23456}\text{F}_5$  shows exclusively a broad  $\text{Cub}_{\text{bi}}$  phase over a range exceeding that of the nonfluorinated compound  $3/\text{H}$  with a smaller apex. This is mainly attributed to

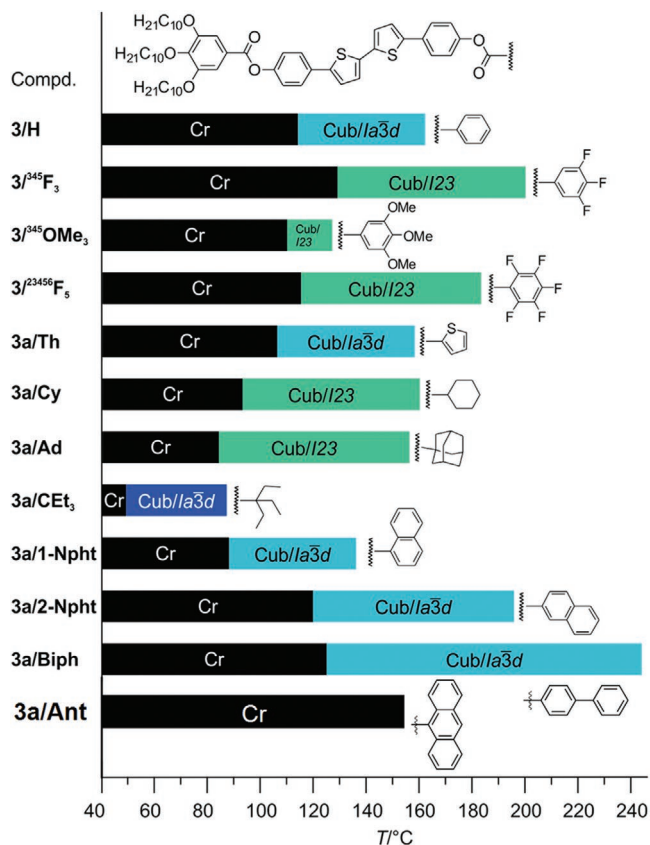


**Figure 7.** Mesophases and transition temperatures of compounds with different types of apex groups on heating; the  $Ia\bar{3}d$  phase of  $3\text{a}/\text{CET}_3$ , indicated by a darker blue represents a short pitch  $Ia\bar{3}d_{(\text{S})}$  phase, whereas all others, shown in light blue belong to the long pitch  $Ia\bar{3}d_{(\text{L})}$ ; for numerical data of  $3/\text{H}$  and  $3/{}^{345}\text{OMe}_3$ , see ref. [87], for compounds  $3\text{a}/\text{Cy}$ ,  $3\text{a}/\text{Ad}$  and  $3\text{a}/\text{CET}_3$ , see ref. [117], for all other data, see Tables S1 and S2 in the Supporting Information).

the electron withdrawing effect of the fluorines, increasing the polar core–core interactions. That the steric effect of fluorination is moderate is indicated by the fact that only the  $I23$  phase, but not the short pitch  $Ia\bar{3}d_{(\text{S})}$  phase is observed for the polyfluorinated compounds. Thus, the taper-shaped tricaténars tolerate multiple substitutions at the apex, allowing easy access to  $\pi$ -systems with distinct electronic properties, while retaining their organization in a well-defined 3D network with cubic symmetry. The major general trends provided by the different apex structures and their substitution patterns are summarized in Figure 8.

## 3.3. Tailoring the Cubic Phases by Heterocyclic, Polycyclic Aromatic, and Alicyclic Units at the Apex (Compounds $3\text{a}/\text{Y}$ )

### 3.3.1. Heterocycles and Alicycles at the Apex

Whereas no effect of replacement of benzene at the apex by thiophene is observed, replacing benzene by cyclohexane changes the cubic phase type from  $Ia\bar{3}d$  to  $I23$ , indicating that the aliphatic ring acts as a larger substituent, especially



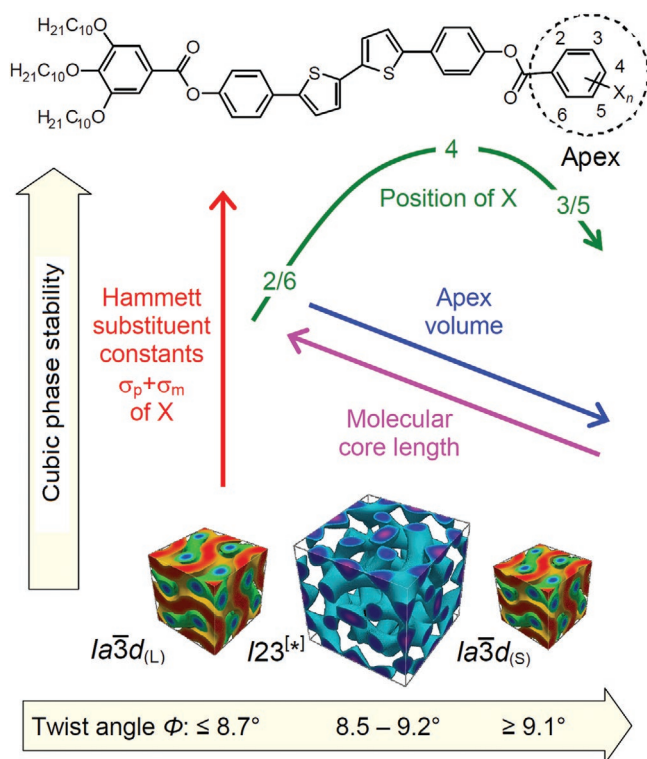


**Figure 8.** Summary of the relations between molecular structure, helical twist, cubic phase type, and cubic phase stability of compounds  $3^m/Y$ , and  $3a/Y$ ; the slight overlap of the helical twist angles results from uncertainties in the determination of the molecular volumes by the used increments<sup>[130]</sup> and possible effects of electrostatic core–core interactions, additionally contributing to the self-assembly.

due to the additional axial H-atoms which change the flat aromatic ring into a bulky substituent expanded in all three spatial dimensions (Figure 7 and Table 2). It is remarkable that even for the large polycyclic adamantyl group ( $3a/Ad$ ), the  $I23$  phase is retained with almost the same  $Cub_{bi}$ -Iso transition temperature as for the cyclohexyl-substituted compound  $3a/Cy$ .<sup>[117]</sup> Even the triethylacetate  $3a/CET_3$ , which can be considered as a noncyclic ring-opened relative of the adamantane compound  $3a/Ad$ , forms a cubic phase, though with reduced stability.<sup>[117]</sup> That these large substituents at the apex cannot remove the cubic phase confirms once more the robustness of this molecular design concept. In contrast to  $3a/Ad$  with an  $I23$  phase, the cubic phase of  $3a/CET_3$  has an  $Ia\bar{3}d$  space group. The small cubic lattice parameter of  $3a/CET_3$  ( $a_{cub} = 8.85$  nm) and the large twist ( $\Phi = 10.1^\circ$ ) are in line with a short pitch  $Ia\bar{3}d_{(S)}$  phase, which is confirmed by the induction of a chiral  $I23$  phase in the contact region with the  $Ia\bar{3}d_{(L)}$  phase of  $3/H$  (see Figure S6 in the Supporting Information). It shows that the triethylacetate group of  $3a/CET_3$  acts as an even larger substituent than adamantane. The larger effective size should be the result of the increased conformational flexibility compared to adamantane, allowing more bulky conformations to be involved in the equilibrium. The change of the cubic phase type upon increasing the cycloaliphatic ring size from cyclobutyl to cyclododecyl is described in more detail in a previous communication.<sup>[117]</sup> Overall, these bulky aliphatic apex structures have

a strong steric effect on mesophase stability, as well as a strong effect on network helicity.

### 3.3.2. Condensed Aromatics and Biphenyl at the Apex

Broad regions of the  $Ia\bar{3}d_{(L)}$  phase were found for the two naphthalene derivatives, where the higher transition temperatures were observed for the 2-naphthoic acid derivative with the naphthyl group arranged colinear with the rod-like core (Figure 7). By contrast, the side-on attached 1-substituted naphthalene leads to a reduction of the cubic phase stability and the anthracene-9-carboxylate  $3a/Anth$  with two laterally annulated benzene rings does not show any LC phase (Figure 7). Based on the calculated twist angles  $\Phi$  (Table 2) and in line with the results of the optical investigation of the contact regions with the  $Ia\bar{3}d_{(L)}$  and  $Ia\bar{3}d_{(S)}$  phases of related compounds (see Figures S7 and S8 and the additional discussions in Section S14.3 in the Supporting Information), the cubic phase of compounds  $3a/1-Npht$ ,  $3a/2-Npht$ , and  $3a/Biph$  is of the same long pitch  $Ia\bar{3}d_{(L)}$  type. Elongation of the rod-like core by the coaxial 2-naphthyl unit, or by replacing the single benzene ring by a linear biphenyl unit stabilizes the cubic phase (Figure 7), increases the lattice parameter, and reduces the twist angle between adjacent molecules along the networks segment if compared to  $3/H$  (Table 2). Overall, there is a very different behavior of aromatic and cycloaliphatic<sup>[117]</sup> end groups. The flat and rigid aromatics contribute to the length and volume of the core unit and thus reduce the twist angle between the cores, retaining the  $Ia\bar{3}d_{(L)}$  phase. By contrast, aliphatic and cycloaliphatic units tend to segregate from the core and contribute to the space filling in the aliphatic periphery, thus increasing the twist, disfavoring the  $Ia\bar{3}d_{(L)}$  and tending toward  $I23$  and ultimately to  $Ia\bar{3}d_{(S)}$ .

## 3.4. Discussion of Cubic Self-Assembly and Mirror Symmetry Breaking in Relation to the Molecular Structure

### 3.4.1. Helical Twist and Cubic Phase Formation

The lateral distance between the two networks in the  $Ia\bar{3}d$  phase, corresponding to the distance between the minimal surfaces, and calculated as  $d_{net} = \sqrt{3}a_{cub}/4 = 4.7\text{--}4.8$  nm, is only a little bit larger than  $L_{mol}$  (4.4–4.6 nm for most compounds). The antiparallel organization of the molecules with full intercalation of the rod-like cores (Figure 3b) would lead to a length of these pairs of around 6.1 nm. The difference to  $d_{net}$  is considered to be due to partial alkyl chain intercalation and chain folding to efficiently fill the space around the networks. The interfacial curvature provided by the 2:3 ratio of core to alkyl chain cross-sectional areas at the interfaces in this organization of the 3/0 tricaténars (Figure 9b,c) appears to be just right for the formation of  $Cub_{bi}$  phases. A larger 2:4 ratio is obtained for the tetracatenars (Figure 9d,e). Though the 3/1 tetracatenars (Figure 9d) form predominately  $Cub_{bi}$  phases too, the symmetric 2/2 tetracatenars (Figure 9e) are much more sensitive to structural modifications and have, if any, only small  $Cub_{bi}$  ranges beside the dominant lamellar and columnar phases.<sup>[69,116,120–124]</sup> One may argue that, on average, rafts of antiparallel 3/1 tetracatenars are equivalent to those of 2/2

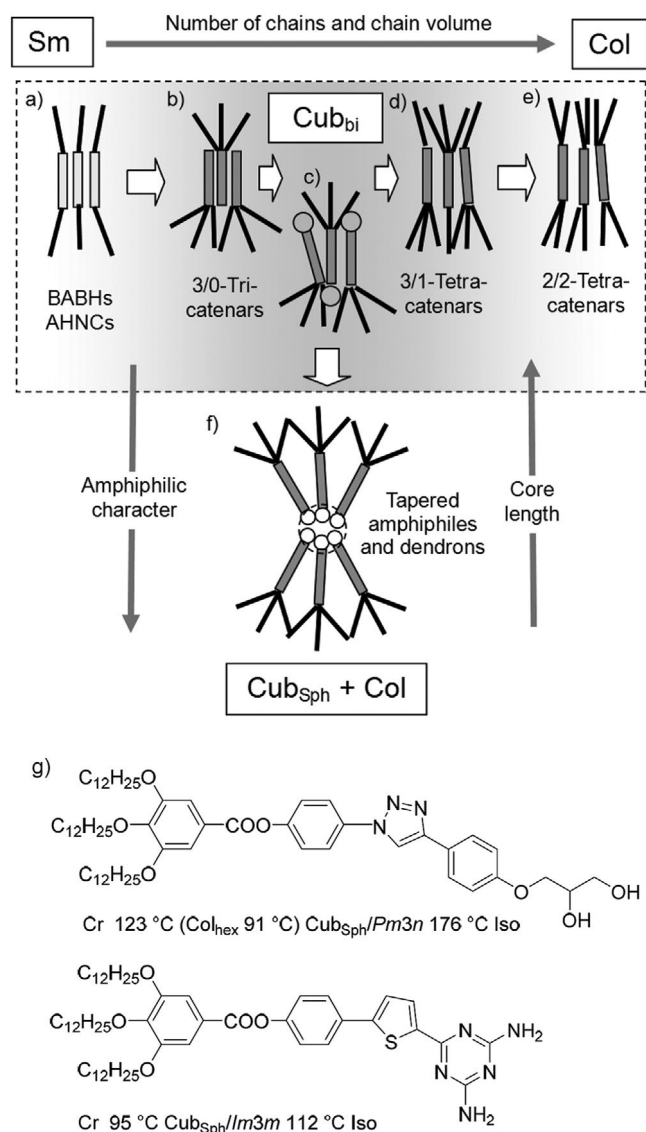


**Figure 9.** a–e) Sketches of self-assembly of cubogenic rod-like molecules depending on the molecular structure (cross-sections of the ribbon-like or columnar segments of the networks). The compounds reported herein belong to types (b–d); f) shows the organization of amphiphilic tapered molecules and g) examples of taper-shaped tricatennars forming micellar (spheroidal) cubic phases (Cub<sub>Sph</sub>).

tetracatenars. However, as the ribbon winds its way through the surrounding of other twisted ribbons, its immediate environment changes and while at one point a symmetric arrangement may be ideal, at other points, more chains may be needed on one side of the ribbon than on the other to plug a local void. Symmetric polycatenars cannot adjust to such local steric requirements. However, it is surprising that such a huge variety of different types of apex substitution, even involving extremely bulky groups as adamantane (3a/Ad), pentafluorobenzene (3/<sup>23456</sup>F<sub>5</sub>), naphthalene (3a/1-Npht), and highly branched alkyl chains (3a/CEt<sub>3</sub>) can lead to such broad temperature ranges of Cub<sub>bi</sub> network phases (Figure 7). It appears that these bulky end groups, favoring the helical twist, allow a denser molecular packing due to an at least

partial synchronization of the overall helical molecular conformers.<sup>[86,95,96,138]</sup> This seems to provide an additional advantage compared to competing lamellar phases, disfavoring the twist, and the columnar phases, having only short range helix correlation.<sup>[95,96,139,140]</sup> If the enthalpic gain of uniform helix packing, provided by the long range transmission of helicity by network formation, exceeds the entropic penalty of chirality synchronization, then the Cub<sub>bi</sub> networks can be additionally stabilized over the competing lamellar and columnar modes of self-assembly. It appears that this Cub<sub>bi</sub> phase stabilizing effect of polyaromatic cores is more general. For example, robust bicontinuous cubic phases were even found for polyaromatic rods with only two alkyl chains (Figure 9a, e.g., BABHs<sup>[107,108]</sup> and the hydrogen-bonded dimers of the ANBCs, see Figure 1c,d).<sup>[16,101,103,104]</sup> In these cases, alkyl chain intercalation or replacing the alkyl chains by perfluorinated chains<sup>[141,142]</sup> or by adding bulky silyl groups<sup>[74,108]</sup> provides the required interfacial curvature for Cub<sub>bi</sub> phase formation. Permanent molecular chirality can further support the helical twist, leading to a series of chirality frustrated LC phases.<sup>[53–55,143]</sup> This contribution of helical packing to Cub<sub>bi</sub> phase stabilization is absent for flexible amphiphilic molecules<sup>[7]</sup> and their dendritic<sup>[18,144]</sup> and polymeric analogs (block copolymers)<sup>[10]</sup> which limits their capability of Cub<sub>bi</sub> phase formation to narrower ranges and this explains the unexpected Cub<sub>bi</sub> phase stability of properly designed rod-like compounds.

Polar substituents like CN and NO<sub>2</sub> with the highest polarity and electron acceptor properties (large  $\sigma_m$  and  $\sigma_p$  Hammett constants, see Table 1 and Table S11 in the Supporting Information) show an especially strong stabilizing effect on the cubic phases due to dipolar interactions and the strengthening of the electrostatic interactions between the electron-rich trialkoxylated and the electron-poor CN-/NO<sub>2</sub>-substituted ends. It appears that polar 3- and 4-substitutions favor a dense packing and increase the intermolecular twist, whereas 2-substitution predominately favors intramolecular twist and reduces the core packing density for steric reasons, thus favoring a transition to lamellar phases (Figure 8). However, only the double *ortho*-substitution of the apex in 3/<sup>26</sup>F<sub>2</sub> and the lateral annulation by two benzene rings in compound 3a/Anth can remove the cubic phases completely.

Further increasing the polarity of the apex substituents, as for example, by introduction of ionic groups or hydrogen bonding groups has the opposite effect and leads, as shown previously, to hexagonal columnar and micellar cubic phases (Cub<sub>Sph</sub>), even for compounds with a long rigid core (Figure 9g).<sup>[145–152]</sup> In all these cases, the segregation of the polar apex from the aromatic cores sets in, which inhibits the antiparallel side-by-side packing of the aromatic cores (Figure 9f). This changes the ratio of aromatic to aliphatic cross-section areas from 2:3 to 1:3, leading to a much stronger interfacial curvature, favoring columnar and micellar self-assembly. Similarly, reducing the rod length and thus increasing the taper angle supports higher interfacial curvature, too.<sup>[18–21,75,144,145,153]</sup>

#### 3.4.2. Helical Twist and the $1a\bar{3}d_{(L)}-123-1a\bar{3}d_{(S)}$ – Cubic Phase Sequence

For the tapered 3/0 tricatennars reported herein, there is a strong dependence of the space group on the size and position of the

substituent(s) at the apex, leading to the sequence  $Ia\bar{3}d_{(L)} \rightarrow I23 \rightarrow Ia\bar{3}d_{(S)}$  with apex size expansion (Figure 8).<sup>[132]</sup> In line with the double network structure of the  $Ia\bar{3}d$  phase and a triple network structure of the  $I23$  phase, the lattice parameter increases by about  $50 \pm 10\%$  at the  $Ia\bar{3}d_{(L)}$ -to- $I23$  transitions. However, within the  $Ia\bar{3}d$  and the  $I23$  phases, the cubic lattice parameter is almost independent of the size of the apex substituent. There is obviously a compensation of the increasing molecular volume, tending to increase  $a_{\text{cub}}$ , opposed by the increasing twist angle between successive rafts and decreasing the number of molecules in a raft, both contributing to a reduction in  $a_{\text{cub}}$  (Tables 1 and 2 and Table S10 in the Supporting Information). Because the molecules in the twisted ribbons must arrive almost perpendicular to the plane of the network junction, a frustration arises between optimal helical pitch and the junction distance. At the same time, the twist angle  $\Phi$  between successive rafts is a compromise between  $\Phi$ -increasing tendency of the clashing end groups and the  $\Phi$ -reducing tendency of the rod-like cores, which prefer to lie parallel and maximize their  $\pi$ - $\pi$  interaction. Another contribution comes from the diastereomeric relation and coupling between supra-molecular helical twist and transient molecular helicity. All these affect the choice of the cubic phase type.<sup>[87,95]</sup> Each structure in the sequence  $Ia\bar{3}d_{(L)}$ - $I23$ - $Ia\bar{3}d_{(S)}$  represents the solution best suited to accommodate a certain range of the twist angle  $\Phi$ . With increasing apex size, the increasing  $\Phi$  reaches up to about  $8.7^\circ$  for the long pitch  $Ia\bar{3}d_{(L)}$  phase,  $8.5^\circ$ - $9.2^\circ$  for the  $I23$  phase, and  $\geq 9.1^\circ$  for the short pitch  $Ia\bar{3}d_{(S)}$  phase (see Figure 8, Tables 1 and 2, and Table S10 in the Supporting Information). These values refer to molecules involving the bisbenzoylated 5,5'-diphenyl-2,2'-bithiophene core unit. They can deviate from these values, for example, if the alkyl chain at the apex is especially long ( $X = \text{OC}_{10}\text{H}_{21}$ ), or as the length and shape of the core is changed, though the fundamental phase sequence remains the same.<sup>[117]</sup> Depending on the contribution of the substituent to the volume effect and the twist, the lattice parameter can increase, as observed for the BABHs and ANBCs,<sup>[101,103,104,107,108]</sup> remain almost constant, as reported here for compounds  $3^m\text{X}_n$  and  $3a/Y$ , or even decreases with increasing volume of the substituents, as recently reported for benzil-based polycatenars.<sup>[154]</sup> However, in all cases, the twist angle increases with the apex volume, leading to the sequence  $Ia\bar{3}d_{(L)}$ - $I23$ - $Ia\bar{3}d_{(S)}$ . While the cubic phase destabilizing steric effect of apex substitution increases from the 4- via the 3- to the 2-position, the effect on the  $\text{Cub}_{\text{bi}}$  phase structure is the largest for the sidewise-directed lateral 3-position and is smaller for the inward-directed lateral 2- and the terminal 4-position (Figure 8).

## 4. Summary and Conclusions

Overall, the concept of taper-shaped 3/0 tricaténars, involving an extended rod-like unit, represents a new robust platform for the design of LC network structures with cubic symmetry. In most cases, the  $\text{Cub}_{\text{bi}}$  phases ( $Ia\bar{3}d$  and  $I23$ ), representing interwoven networks with 3-way junctions, are the only observed LC phases in wide temperature ranges and for a wide variety of groups attached to the apex, including perfluorinated aromatics, heteroaromatics, alicyclic and polycyclic rings, and even for highly

branched chains (Figures 3, 4, 6–8). Often, these network phases are stable down to ambient temperature (Tables S1 and S2, Supporting Information). An organization with locally adjustable antiparallel side-by-side packing of the rod-like cores, leading to a 2:3 average ratio of core-to-chain width (Figures 3b and 9b,c), is proposed to be responsible for the robustness of the  $\text{Cub}_{\text{bi}}$  phases and their strongly preferred formation over lamellar and columnar modes of organization. The chirality-synchronized helical packing in the networks is thought to additionally stabilize the cubic phases by allowing a denser molecular packing. The observed insensitivity of cubic network formation to apex substitution by a large diversity of functional groups allows tuning of the electronic properties (HOMO–LUMO bandgap) of the  $\pi$ -conjugated rod-like cores organized in the helical networks. This potential for application as functional materials is augmented by the possibility of switching between an achiral ( $Ia\bar{3}d$ ) and chiral ( $I23$ ) state. With increasing size of the apex the sequence  $Ia\bar{3}d_{(L)}$ - $I23$ - $Ia\bar{3}d_{(S)}$  is observed which appears to be universal and is explained by an increasing helical twist along the networks (see Figure 8, Tables 1 and 2, and Table S10 in the Supporting Information). The long pitch and short pitch  $Ia\bar{3}d$  phases are considered as distinct ranges of the same macroscopically achiral gyroid double network phase, which is interrupted for a certain twist angle range by the homochiral triple network  $I23$  phase (Figure 8). The helical twist angle can be adjusted by design of the individual molecules or, alternatively, by mixing short and long pitch  $Ia\bar{3}d$  phases (Figure 5).

Overall, this work provides a general understanding of supra-molecular self-assembly in  $\text{Cub}_{\text{bi}}$  network phases depending on details of the molecular structure and thus paves the way to the directed design of cubogenic and spontaneously chiral functional materials with tunable application-relevant properties. More generally, it provides insights into the process of spontaneous mirror symmetry breaking in soft matter,<sup>[95,96,136,155]</sup> and it shows the importance of network formation for this process. Spontaneous emergence of chirality during self-assembly is also of paramount interest for circularly-polarized emission<sup>[46–48]</sup> and photonic applications,<sup>[27,28]</sup> and for new dynamic routes to absolute enantioselective synthesis.<sup>[156–158]</sup>

## Supporting Information

Supporting Information is available from the Wiley Online Library or from the author.

## Acknowledgements

C.D. and T.R. contributed equally to this work. For support with synchrotron experiments, the authors are grateful to Dr. O. Shebanova and Prof. N. Terill at station I22, Diamond Light Source, and Dr. O. Bikondoa and Dr. P. Thompson at the EPSRC-funded XMaS beam line at ESRF. Financial support is acknowledged from the 111 Project 2.0 of China (Grant No. BP2018008) and from the EPSRC (Grant Nos. EP-P002250, EP-T003294). Open access funding enabled and organized by Projekt DEAL.

## Conflict of Interest

The authors declare no conflict of interest.

## Keywords

bicontinuous cubic phases, chirality, helical superstructures, liquid crystals, mirror symmetry breaking, self-assembly, supramolecular networks

Received: May 20, 2020

Revised: July 6, 2020

Published online: August 11, 2020

- [1] S. Otto, *Acc. Chem. Res.* **2012**, *45*, 2200.
- [2] B. A. Grzybowski, K. Fitzner, J. Paczesny, S. Granick, *Chem. Soc. Rev.* **2017**, *46*, 5647.
- [3] M. O'Keeffe, O. M. Yaghi, *Chem. Rev.* **2012**, *112*, 675.
- [4] S. Hyde, S. Andersson, K. Larsson, Z. Blum, T. Landh, S. Lidin, B. W. Ninham, *The Language of Shape: The Role of Curvature in Condensed Matter: Physics, Chemistry and Biology*, Elsevier, Amsterdam **1997**.
- [5] M. L. Lynch, P. T. Spicer, *Bicontinuous Liquid Crystals*, Surfactant Science Series, Vol. 127, CRC Press – Taylor & Francis Group, Boca Raton, FL, USA **2005**.
- [6] V. Luzzati, R. Vargas, P. Mariani, A. Gulik, H. Delacroix, *J. Mol. Biol.* **1993**, *229*, 540.
- [7] J. M. Seddon, R. H. Templer, in *Handbook of Biological Physics*, Vol. 1 (Eds: R. Lipowsky, E. Sackmann), Elsevier, Amsterdam **1995**, pp. 97–160.
- [8] G. L. Jackson, D. V. Perroni, M. K. Mahanthappa, *J. Phys. Chem. B* **2017**, *121*, 9429.
- [9] M. A. Shcherbina, A. V. Bakirova, A. N. Yakunin, V. Percec, U. Beginn, M. Möller, S. N. Chvalun, *Crystallogr. Rep.* **2012**, *57*, 151.
- [10] A. J. Meuler, M. A. Hillmyer, F. S. Bates, *Macromolecules* **2009**, *42*, 7221.
- [11] S. Diele, P. Göring, in *Handbook of Liquid Crystals*, Vol. 2B (Eds: D. Demus, J. Goodby, G. W. Gray, H.-W. Spiess, V. Vill), Wiley-VCH, Weinheim, Germany **1998**, pp. 887–900.
- [12] S. Diele, *Curr. Opin. Colloid Interface Sci.* **2002**, *7*, 333.
- [13] M. Imperor-Clerc, *Curr. Opin. Colloid Interface Sci.* **2005**, *9*, 370.
- [14] G. Ungar, F. Liu, X. Zeng, in *Handbook of Liquid Crystals*, Vol. 5, 2nd ed. (Eds: J. W. Goodby, P. J. Collings, T. Kato, C. Tschierske, H. F. Gleeson, P. Raynes), Wiley-VCH, Weinheim **2014**, pp. 363–436.
- [15] C. Tschierske, *Angew. Chem., Int. Ed.* **2013**, *52*, 8828.
- [16] C. Tschierske, *J. Mater. Chem.* **2001**, *11*, 2647.
- [17] S. Kutsumizu, *Isr. J. Chem.* **2012**, *52*, 844.
- [18] S. N. Chvalun, M. A. Shcherbina, A. N. Yakunin, J. Blackwell, V. Percec, *Polym. Sci., Ser. A* **2007**, *49*, 158.
- [19] K. Borisch, S. Diele, P. Göring, C. Tschierske, *Chem. Commun.* **1996**, 237.
- [20] K. Borisch, S. Diele, P. Göring, H. Kresse, C. Tschierske, *J. Mater. Chem.* **1998**, *8*, 529.
- [21] K. Borisch, C. Tschierske, P. Göring, S. Diele, *Chem. Commun.* **1998**, 2711.
- [22] L. van 't Hag, S. L. Gras, C. E. Conn, C. J. Drummond, *Chem. Soc. Rev.* **2017**, *46*, 2705.
- [23] H. M. G. Barriga, M. N. Holme, M. M. Stevens, *Angew. Chem., Int. Ed.* **2019**, *58*, 2958.
- [24] C. E. Conn, C. J. Drummond, *Soft Matter* **2013**, *9*, 3449.
- [25] M. Antonietti, *Philos. Trans. R. Soc., A* **2006**, *364*, 2817.
- [26] N. Marets, D. Kuo, J. R. Torrey, T. Sakamoto, M. Henmi, H. Katayama, T. Kato, *Adv. Healthcare Mater.* **2017**, *6*, 1700252.
- [27] K. Bisoyi, T. J. Bunning, Q. Li, *Adv. Mater.* **2018**, *30*, 1706512.
- [28] H.-Y. Hsueh, Y.-C. Ling, H.-F. Wang, L.-Y. C. Chien, Y.-C. Hung, E. L. Thomas, R.-M. Ho, *Adv. Mater.* **2014**, *26*, 3225.
- [29] L. Han, S. Che, *Adv. Mater.* **2018**, *30*, 1705708.
- [30] W. Pisula, M. Zorn, J. Y. Chang, K. Müllen, R. Zentel, *Macromol. Rapid Commun.* **2009**, *30*, 1179.
- [31] M. Funahashi, *J. Mater. Chem. C* **2014**, *2*, 7451.
- [32] Y. Shimizu, K. Oikawa, K.-i. Nakayama, D. Guillon, *J. Mater. Chem.* **2007**, *17*, 4223.
- [33] M. Funahashi, H. Shimura, M. Yoshio, T. Kato, *Struct. Bonding* **2008**, *128*, 151.
- [34] J. Hanna, A. Ohno, H. Iino, *Thin Solid Films* **2014**, *554*, 58.
- [35] M. Kumar, S. Kumar, *Polym. J.* **2017**, *49*, 85.
- [36] S. Sergeyev, W. Pisula, Y. H. Geerts, *Chem. Soc. Rev.* **2007**, *36*, 1902.
- [37] T. Kobayashi, Y.-X. Li, A. Ono, X.-B. Zeng, T. Ichikawa, *Chem. Sci.* **2019**, *10*, 6245.
- [38] T. Kobayashi, T. Ichikawa, T. Kato, H. Ohno, *Adv. Mater.* **2017**, *29*, 1604429.
- [39] H. Zhang, L. Li, M. Möller, X. Zhu, J. J. Hernandez Rueda, M. Rosenthal, D. A. Ivanov, *Adv. Mater.* **2013**, *25*, 3543.
- [40] T. Kato, M. Yoshio, T. Ichikawa, B. Soberats, H. Ohno, M. Funahashi, *Nat. Rev. Mater.* **2017**, *2*, 17001.
- [41] T. Kato, J. Uchida, T. Ichikawa, T. Sakamoto, *Angew. Chem., Int. Ed.* **2018**, *57*, 4355.
- [42] T. Ichikawa, M. Yoshio, A. Hamasaki, S. Taguchi, F. Liu, X. B. Zeng, G. Ungar, H. Ohno, T. Kato, *J. Am. Chem. Soc.* **2012**, *134*, 2634.
- [43] E. J. W. Crossland, M. Kamperman, M. Nedelcu, C. Ducati, U. Wiesner, D.-M. Smilgies, G. E. S. Toombes, M. A. Hillmyer, S. Ludwigs, U. Steiner, H. J. Snaith, *Nano Lett.* **2009**, *9*, 2807.
- [44] J.-M. Suisse, H. Mori, H. Monobe, S. Kutsumizu, Y. Shimizu, *Soft Matter* **2011**, *7*, 11086.
- [45] G. Park, K. Goossens, T. J. Shin, C. W. Bielawski, *Chem. - Eur. J.* **2018**, *24*, 6399.
- [46] F. Song, Z. Zhao, Z. Liu, J. W. Y. Lam, B. Z. Tang, *J. Mater. Chem. C* **2020**, *8*, 3284.
- [47] Y. Sang, J. Han, T. Zhao, P. Duan, M. Liu, *Adv. Mater.* **2019**, 1900110.
- [48] Anuradha, D. D. La, M. Al Kobaisi, A. Gupta, S. V. Bhosale, *Chem. Eur. J.* **2017**, *23*, 3950.
- [49] Only recently single network Cub LC phases have been predicted and first examples have been experimentally observed.<sup>[57,58]</sup>
- [50] Besides the rod-like segments, also bent and disk-like units can lead to Cub phases in few cases.
- [51] A.-M. Levelut, C. Germain, P. Keller, L. Liebert, J. Billard, *J. Phys.* **1983**, *44*, 623.
- [52] A.-M. Levelut, M. Clerc, *Liq. Cryst.* **1998**, *24*, 105.
- [53] M. Yoneya, *Chem. Rec.* **2011**, *11*, 66.
- [54] T. Yamamoto, I. Nishiyama, M. Yoneya, H. Yokoyama, *J. Phys. Chem. B* **2009**, *113*, 11564.
- [55] I. Nishiyama, *Chem. Rec.* **2009**, *9*, 340.
- [56] H. Lu, X. Zeng, G. Ungar, C. Dressel, C. Tschierske, *Angew. Chem., Int. Ed.* **2018**, *57*, 2835.
- [57] X. Zeng, S. Poppe, A. Lehmann, M. Prehm, C. Chen, F. Liu, H. Lu, G. Ungar, C. Tschierske, *Angew. Chem.* **2019**, *131*, 7453.
- [58] S. Poppe, X. Cheng, C. Chen, X. Zeng, R.-B. Zhang, F. Liu, G. Ungar, C. Tschierske, *J. Am. Chem. Soc.* **2020**, *142*, 3296.
- [59] A. J. Mukhtyar, F. A. Escobedo, *Macromolecules* **2018**, *51*, 9781.
- [60] F. Liu, M. Prehm, X. B. Zeng, C. Tschierske, G. Ungar, *J. Am. Chem. Soc.* **2014**, *136*, 6846.
- [61] S. Poppe, C. Chen, F. Liu, C. Tschierske, *Chem. Commun.* **2018**, *54*, 11196.
- [62] X. B. Zeng, M. Prehm, G. Ungar, C. Tschierske, F. Liu, *Angew. Chem., Int. Ed.* **2016**, *55*, 8324.
- [63] M. Poppe, C. Chen, F. Liu, S. Poppe, C. Tschierske, *Chem. - Eur. J.* **2017**, *23*, 7196.
- [64] M. Poppe, C. Chen, H. Ebert, S. Poppe, M. Prehm, C. Kerzig, F. Liu, C. Tschierske, *Soft Matter* **2017**, *13*, 4381.
- [65] C. Chen, R. Kieffer, H. Ebert, M. Prehm, R.-B. Zhang, X. Zeng, F. Liu, G. Ungar, C. Tschierske, *Angew. Chem., Int. Ed.* **2020**, *59*, 2725.

- [66] Cub phases with the molecules organized on the minimal surfaces in the middle of the continuum between the networks are rare; there are also rod-like molecules having laterally alkyl-substituted rods, forming  $Cub_{bi}$  phases with the rods aligned parallel to the networks<sup>[57,58,60–62]</sup> or parallel to the minimal surfaces.<sup>[65]</sup>
- [67] B.-K. Cho, A. Jain, S. M. Gruner, U. Wiesner, *Science* **2004**, 305, 1598.
- [68] I. Bury, B. Heinrich, C. Bourgogne, D. Guillon, B. Donnio, *Chem. - Eur. J.* **2006**, 12, 8396.
- [69] D. W. Bruce, *Acc. Chem. Res.* **2000**, 33, 831.
- [70] K. Hatsusaka, K. Ohta, I. Yamamoto, H. Shirai, *J. Mater. Chem.* **2001**, 11, 423.
- [71] M.d. A. Alam, J. Motoyanagi, Y. Yamamoto, T. Fukushima, J. Kim, K. Kato, M. Takata, A. Saeki, S. Seki, S. Tagawa, T. Aida, *J. Am. Chem. Soc.* **2009**, 131, 17722.
- [72] K. Hatsusaka, M. Kimura, K. Ohta, *Bull. Chem. Soc. Jpn.* **2003**, 76, 781.
- [73] P. Massiot, M. Imperor-Clerc, M. Veber, R. Deschenaux, *Chem. Mater.* **2005**, 17, 1946.
- [74] E. Nishikawa, E. T. Samulski, *Liq. Cryst.* **2000**, 27, 1463.
- [75] X. Cheng, M. K. Das, S. Diele, C. Tschierske, *Langmuir* **2002**, 18, 6521.
- [76] R. A. Reddy, U. Baumeister, C. Keith, H. Hahn, H. Lang, C. Tschierske, *Soft Matter* **2007**, 3, 558.
- [77] S. Kang, M. Harada, X. Li, M. Tokita, J. Watanabe, *Soft Matter* **2012**, 8, 1916.
- [78] J. Matraszek, J. Zapala, J. Mieczkowski, D. Pocięcha, E. Gorecka, *Chem. Commun.* **2015**, 51, 5048.
- [79] M. Lee, B.-K. Cho, H. Kim, J.-Y. Yoon, W.-C. Zin, *J. Am. Chem. Soc.* **1998**, 120, 9168.
- [80] M. Lee, Y.-S. Yoo, *J. Mater. Chem.* **2002**, 12, 2161.
- [81] W. T. Gozdz, R. Holyst, *Phys. Rev. E* **1996**, 54, 5012.
- [82] X. Zeng, G. Ungar, M. Imperor-Clerc, *Nat. Mater.* **2005**, 4, 562.
- [83] X. Zeng, L. Cseh, G. H. Mehl, G. Ungar, *J. Mater. Chem.* **2008**, 18, 2953.
- [84] K. Ozawa, Y. Yamamura, S. Yasuzuka, H. Mori, S. Kutsumizu, K. Saito, *J. Phys. Chem. B* **2008**, 112, 12179.
- [85] K. Saito, Y. Yamamura, Y. Miwa, S. Kutsumizu, *Phys. Chem. Chem. Phys.* **2016**, 18, 3280.
- [86] C. Dressel, T. Reppe, M. Prehm, M. Brautzsch, C. Tschierske, *Nat. Chem.* **2014**, 6, 971.
- [87] C. Dressel, F. Liu, M. Prehm, X. B. Zeng, G. Ungar, C. Tschierske, *Angew. Chem., Int. Ed.* **2014**, 53, 13115.
- [88] C. Dressel, W. Weissflog, C. Tschierske, *Chem. Commun.* **2015**, 51, 15850.
- [89] M. Alaasar, M. Prehm, Y. Cao, F. Liu, C. Tschierske, *Angew. Chem., Int. Ed.* **2016**, 55, 312.
- [90] M. Alaasar, S. Poppe, Q. Dong, F. Liu, C. Tschierske, *Chem. Commun.* **2016**, 52, 13869.
- [91] M. Alaasar, S. Poppe, Q. Dong, F. Liu, C. Tschierske, *Angew. Chem., Int. Ed.* **2017**, 56, 10801.
- [92] The first report on mirror symmetry breaking in cubic phases came from Kishikawa and co-workers,<sup>[93]</sup> though the structure of the cubic phase and the origin of chirality were unclear at that time.
- [93] T. Kajitani, S. Kohmoto, M. Yamamoto, K. Kishikawa, *Chem. Mater.* **2005**, 17, 3812.
- [94] H. R. Brand, H. Pleiner, *Eur. Phys. J. E: Soft Matter Biol. Phys.* **2019**, 42, 142.
- [95] C. Tschierske, G. Ungar, *ChemPhysChem* **2016**, 17, 9.
- [96] C. Tschierske, *Liq. Cryst.* **2018**, 45, 2221.
- [97] A twist in the organization of the  $la\bar{3}d$  phase was first discussed by Kutsumizu and co-workers.<sup>[98]</sup>
- [98] Y. Nakazawa, Y. Yamamura, S. Kutsumizu, K. Saito, *J. Phys. Soc. Jpn.* **2012**, 81, 094601.
- [99] X. B. Zeng, G. Ungar, *J. Mater. Chem. C* **2020**, 8, 5389.
- [100] G. W. Gray, B. Jones, F. Marson, *J. Chem. Soc.* **1957**, 393.
- [101] D. Demus, G. Kunicke, J. Neelsen, H. Z. Sackmann, *Z. Naturforsch., A: Phys. Sci.* **1968**, 23, 84.
- [102] S. Kutsumizu, T. Ichikawa, M. Yamada, S. Nojima, S. Yano, *J. Phys. Chem. B* **2000**, 104, 10196.
- [103] S. Kutsumizu, K. Morita, T. Ichikawa, S. Yano, S. Nojima, T. Yamaguchi, *Liq. Cryst.* **2002**, 29, 1447.
- [104] S. Kutsumizu, K. Morita, S. Yano, S. Nojima, *Liq. Cryst.* **2002**, 29, 1459.
- [105] H. Schubert, J. Hauschild, D. Demus, S. Hoffmann, *Z. Chem.* **1978**, 18, 256.
- [106] D. Demus, A. Gloza, H. Hartung, A. Hauser, I. Rapthel, A. Wiegeleben, *Cryst. Res. Technol.* **1981**, 16, 1445.
- [107] S. Kutsumizu, H. Mori, M. Fukatami, S. Naito, K. Sakajiri, K. Saito, *Chem. Mater.* **2008**, 20, 3675.
- [108] S. Kutsumizu, Y. Yamada, T. Sugimoto, N. Yamada, T. Udagawa, Y. Miwa, *Phys. Chem. Chem. Phys.* **2018**, 20, 7953.
- [109] S. Kutsumizu, I. Tokiwa, A. Kawafuchi, Y. Miwa, Y. Yamamura, K. Saito, *Phys. Chem. Chem. Phys.* **2016**, 18, 9013.
- [110] P. Göring, S. Diele, S. Fischer, A. Wiegeleben, G. Pelzl, H. Stegemeyer, W. Thyen, *Liq. Cryst.* **1998**, 25, 467.
- [111] S. Kutsumizu, S. Miisako, Y. Miwa, M. Kitagawa, Y. Yamamura, K. Saito, *Phys. Chem. Chem. Phys.* **2016**, 18, 17341.
- [112] M. Vogrin, N. Vaupotic, M. M. Wojcik, J. Mieczkowski, K. Madrak, D. Pocięcha, E. Gorecka, *Phys. Chem. Chem. Phys.* **2014**, 16, 16067.
- [113] B. Pansu, Y. Nastishin, M. Imperor-Clerc, M. Veber, H. T. Nguyen, *Eur. Phys. J. E: Soft Matter Biol. Phys.* **2004**, 15, 225.
- [114] J. M. Wolska, J. Wilk, D. Pocięcha, J. Mieczkowski, E. Gorecka, *Chem. - Eur. J.* **2017**, 23, 6853.
- [115] J. M. Wolska, D. Pocięcha, J. Mieczkowski, E. Gorecka, *Liq. Cryst.* **2016**, 43, 235.
- [116] A. I. Smirnova, B. Heinrich, B. Donnio, D. W. Bruce, *RSC Adv.* **2015**, 5, 75149.
- [117] T. Reppe, C. Dressel, S. Poppe, C. Tschierske, *Chem. Commun.* **2020**, 56, 711.
- [118] a) H. T. Nguyen, C. Destrade, A.-M. Levelut, J. Malthete, *J. Phys.* **1986**, 47, 553; b) A.-M. Levelut, Y. Fang, *Colloq. Phys.* **1990**, 51, C7-229.
- [119] J. Malthete, H. T. Nguyen, C. Destrade, *Liq. Cryst.* **1993**, 13, 171.
- [120] H. T. Nguyen, C. Destrade, J. Malthete, *Adv. Mater.* **1997**, 9, 375.
- [121] H. T. Nguyen, C. Destrade, J. Malthete, in *Handbook of Liquid Crystals*, Vol. 2B (Eds: D. Demus, J. Goodby, G. W. Gray, H.-W. Spiess, V. Vill), Wiley-VCH, Weinheim **1998**, pp. 865–885.
- [122] W. Weissflog, in *Handbook of Liquid Crystals*, Vol. 5, 2nd ed. (Eds: J. W. Goodby, J. P. Collings, T. Kato, C. Tschierske, H. F. Gleeson, P. Raynes), Wiley-VCH, Weinheim **2014**, pp. 89–174.
- [123] D. W. Bruce, S. A. Hudson, *J. Mater. Chem.* **1994**, 4, 479.
- [124] K. E. Rowe, D. W. Bruce, *J. Mater. Chem.* **1998**, 8, 331.
- [125] G. W. Gray, B. M. Warrall, *J. Chem. Soc.* **1959**, 1545.
- [126] A. Mishra, C.-Q. Ma, P. Bäuerle, *Chem. Rev.* **2009**, 109, 1141.
- [127] C. Wang, H. Dong, W. Hu, Y. Liu, C. Zhu, *Chem. Rev.* **2012**, 112, 2208.
- [128] F. C. Spano, *Acc. Chem. Res.* **2010**, 43, 429.
- [129] C. Hansch, A. Leo, R. W. Taft, *Chem. Rev.* **1997**, 97, 2995.
- [130] A. Immirzi, B. Perini, *Acta Crystallogr., Sect. A: Found. Adv.* **1977**, 33, 216.
- [131] Also compound **3/ODec** (Figure 3a) forms the  $I23$  lattice, but this compound is considered as  $3/1$  tetracatenar as the substituent at the apex provides an additional long alkyl chain.
- [132] The phase sequence  $la\bar{3}d-I23-la\bar{3}d$  is the same as previously observed for the ANBCs and BABHs<sup>[17]</sup> and for tricaténars with alicyclic apex upon ring expansion.<sup>[117]</sup>
- [133] A. Pegenau, T. Hegmann, C. Tschierske, S. Diele, *Chem. - Eur. J.* **1999**, 5, 1643.

- [134] This behavior is very similar to that observed for the SmCPR<sup>[6]</sup> phase of bent-core molecules, where the emerging polarization leads to geometrical layer chirality, supporting the twisted organization.<sup>[135]</sup>
- [135] M. Alaasar, M. Prehm, M. Nagaraj, J. K. Vij, C. Tschierske, *Adv. Mater.* **2013**, *25*, 2186.
- [136] H. Takezoe, *Top. Curr. Chem.* **2012**, *318*, 303.
- [137] P. S. Salter, P. W. Benzie, R. A. Reddy, C. Tschierske, S. J. Elston, E. P. Raynes, *Phys. Rev. E* **2009**, *80*, 031701.
- [138] R. P. Lemieux, *Acc. Chem. Res.* **2001**, *34*, 845.
- [139] L. Tauchi, T. Nakagaki, M. Shimizu, E. Itoh, M. Yasutake, K. Ohta, *J. Porphyrins Phthalocyanines* **2013**, *17*, 1080.
- [140] M. Lehmann, M. Hugel, *Angew. Chem., Int. Ed.* **2015**, *54*, 4110.
- [141] E. Nishikawa, J. Yamamoto, H. Yokoyama, *J. Mater. Chem.* **2003**, *13*, 1887.
- [142] A. Yoshizawa, *Polym. J.* **2012**, *44*, 490.
- [143] A.-M. Levelut, E. Hallouin, D. Bennemann, G. Heppke, D. Lttsch, *J. Phys. II* **1997**, *7*, 981.
- [144] B. M. Rosen, C. J. Wilson, D. A. Wilson, M. Peterca, M. R. Imam, V. Percec, *Chem. Rev.* **2009**, *109*, 6275.
- [145] B. M. Rosen, M. Peterca, C. Huang, X. Zeng, G. Ungar, V. Percec, *Angew. Chem., Int. Ed.* **2010**, *49*, 7002.
- [146] S. Lecommandoux, H.-A. Klok, M. Sayar, S. I. Stupp, *J. Polym. Sci., Part A: Polym. Chem.* **2003**, *41*, 3501.
- [147] X. H. Cheng, X. Q. Bai, S. Jing, H. Ebert, M. Prehm, C. Tschierske, *Chem. - Eur. J.* **2010**, *16*, 4588.
- [148] X. H. Cheng, F. W. Su, R. Huang, H. F. Gao, M. Prehm, C. Tschierske, *Soft Matter* **2012**, *8*, 2274.
- [149] H. Dai, X. Yang, X. Tan, F. Su, X. Cheng, F. Liu, C. Tschierske, *Chem. Commun.* **2013**, *49*, 10617.
- [150] X. Tan, L. Kong, H. Dai, X. Cheng, F. Liu, C. Tschierske, *Chem. - Eur. J.* **2013**, *19*, 16303.
- [151] M.-H. Yen, J. Chairapa, X. B. Zeng, Y. Liu, L. Cseh, G. H. Mehl, G. Ungar, *J. Am. Chem. Soc.* **2016**, *138*, 5757.
- [152] X. H. Yao, L. Cseh, X. B. Zeng, M. Xue, Y. S. Liu, G. Ungar, *Nanoscale Horiz.* **2017**, *2*, 43.
- [153] V. Percec, M. Glodde, T. K. Bera, Y. Miura, I. Shiyonovskaya, K. D. Singer, V. S. K. Balagurusamy, P. A. Heiney, I. Schnell, A. Rapp, H.-W. Spiess, S. D. Hudsonk, H. Duank, *Nature* **2002**, *419*, 384.
- [154] T. Reppe, S. Poppe, X. Cai, Y. Cao, F. Liu, C. Tschierske, *Chem. Sci.* **2020**, *11*, 5902.
- [155] D. M. Walba, in *Materials-Chirality, Topics in Stereochemistry*, Vol. 24 (Eds: M. M. Green, R. J. M. Nolte, E. W. Meijer), Wiley, Hoboken, NJ **2003**, pp. 457–518.
- [156] A. Yoshizawa, M. Kurata, *New J. Chem.* **2019**, *43*, 8865.
- [157] N. Uemura, K. Sano, A. Matsumoto, Y. Yoshida, T. Mino, M. Sakamoto, *Chem. - Asian J.* **2019**, *14*, 4150.
- [158] Y. Nagata, R. Takeda, M. Sugimoto, *ACS Cent. Sci.* **2019**, *5*, 1235.